Optical conductivity of a 2DEG with anisotropic Rashba interaction at the interface of $LaAlO_3/SrTiO_3$

Alestin Mawrie and Tarun Kanti Ghosh
Department of Physics, Indian Institute of Technology-Kanpur, Kanpur-208 016, India
(Dated: January 5, 2016)

We study optical conductivity of a two-dimensional electron gas with anisotropic k-cubic Rashba spin-orbit interaction formed at the $LaAlO_3/SrTiO_3$ interface. The anisotropic spin splitting energy gives rise to different features of the optical conductivity in comparison to the isotropic k-cubic Rashba spin-orbit interaction. For large carrier density and strong spin-orbit couplings, the density dependence of Drude weight deviates from the linear behavior. The charge and optical conductivities remain isotropic despite anisotropic nature of the Fermi contours. An infinitesimally small photon energy would suffice to initiate inter-band optical transitions due to degeneracy along certain directions in momentum space. The optical conductivity shows a single peak at a given photon energy depending on the system parameters and then falls off to zero at higher photon energy. These features are lacking for systems with isotropic k-cubic Rashba spin-orbit coupling. These striking features can be used to extract the information about nature of the spin-orbit interaction experimentally and illuminate some light on the orbital origin of the two-dimensional electron gas.

PACS numbers: 78.67.-n, 72.20.-i, 71.70.Ej

I. INTRODUCTION

Spin-orbit interaction[1,2] (SOI) plays an important role in understanding physical properties of different materials as it lifts the spin degeneracy due to the absence of either the structure inversion symmetry or the time reversal symmetry. In general, there are two different types of symmetry dependent SOI, Rashba[3,4] and Dresselhaus[5] SOIs, in various condensed matter systems. In two-dimensional electron gas (2DEG) formed at the III-V semiconductor heterostructures[6] and in various topological insulating systems[7], the Rashba SOI (RSOI) is linear in momentum and of the form $H_R = i\alpha k_- \sigma_+ + \text{h.c.}$, where α is the strength of RSOI, $\sigma_\pm = \sigma_x \pm i\sigma_y$ with σ_x and σ_y are the Pauli's spin matrices and $k_\pm = k_x \pm ik_y$ with k_x and k_y the components of the wave vector $\mathbf{k}$. Besides, the Rashba SOC in two-dimensional hole gas formed at the interface of p-type GaAs/AlGaAs heterostructures[8,9], 2DEG on the surface of $SrTiO_3$ single crystals[10] and in 2D hole gas formed in a strained Ge/SiGe quantum well[11] is cubic in momentum and is of the form $H_R^{\rm iso} = i\alpha k_-^3 \sigma_+ + \text{h.c.}$ The spin splitting energy due to this RSOI is always isotropic and hereafter we will mention this as isotropic cubic Rashba SOC.

An extremely high mobility 2DEG was discovered at the interface of the complex oxides $LaAlO_3$ and $SrTiO_3$[12–14]. The LAO/STO interface structure now has a broken structure inversion symmetry as a result of the confinement along the axis normal to the interface, which leads to the lifting of the spin-degeneracy of the six t_{2g} orbitals in STO[15]. Moreover, the d_{xy} orbitals are confined in the x-y plane and are localized at the interface due to impurities and electron-phonon coupling[16]. Whereas the electrons that contribute to the transports are associated with the d_{xz} and d_{yz} orbitals[16]. One of the major concerns is to understand the nature of the spin-orbit interaction of the charge carriers at the oxide interface. In Refs.[17,18], it is proposed that a k-linear SOC for d_{xy} orbital and an isotropic k-cubic for d_{xz} and d_{yz} orbitals. The magneto-transport measurement of 2DEG at the oxide interface has indicated the existence of k-cubic RSOI and is modeled using the isotropic k-cubic SOI $H_R^{\rm iso}$[10,19]. On the other hand, the first-principle calculations suggested anisotropic non-parabolic spin-split branches for the d_{xz} and d_{yz} orbitals[20]. Two recent polarization-dependent ARPES revealed non-isotropic Fermi contours of the 2DEG at the oxide interface[21]. Very recent theoretical study[22] predicted that these orbitals are characterized by k-cubic but anisotropic Rashba spin-orbit interaction whose form is given by $H_R^{\rm ani} = \alpha(k_x^2 - k_y^2)(\mathbf{k} \times \boldsymbol{\sigma}) \cdot \hat{z}$. The spin splitting energy and Fermi contours become highly anisotropic as a result of this anisotropic SOI. In this paper we will refer this as anisotropic RSOI. This form of the anisotropic RSOI[22] enables to explain the experimental observations of the anisotropic spin susceptibility[23,24] successfully. It is also shown[22] that the anisotropic RSOI leads to different behavior of the spin Hall conductivity, in comparison to the isotropic k-cubic RSOI.

The spectroscopic measurement of the absorptive part of the optical conductivity can probe the spin-split energy levels. Theoretical studies of the optical conductivity of various charged systems with an isotropic k-cubic Rashba SOI have been carried out[25–28,30]. It is shown that the optical transition takes place for a certain range of photon energy depending on the carrier density and spin-orbit coupling constant. At zero temperature, it takes a box-like function and its value is $\sigma_{xx}^{\rm iso} = 3e^2/(16\hbar)$, independent of carrier density and spin-orbit coupling strength.

In this paper we study the Drude weight and optical conductivities of the 2DEG with anisotropic k-cubic RSOI formed at the oxide interface and compare our results with that of the isotropic k-cubic RSOI. Firstly, we present the characteristics of the zero-frequency Drude

weight as a function of the charge density and strength of the anisotropic RSOI. We find that the Drude weight is strongly modified due to the presence of the anisotropic k-cubic SOI. It deviates from the linear density dependence for large carrier density and for strong spin-orbit coupling. The Drude weight decreases with the increase of the strength of RSOI. Secondly, we find that an infinitesimally small photon energy would initiate the interband optical transition. This is due to the vanishing spin-splitting energy along certain directions in the momentum space. There is a single peak in the optical conductivity and its value depends on the electron density and strength of the anisotropic RSOI. Moreover, the charge and optical conductivities are isotropic despite the fact that the RSOI is anisotropic. The van Hove singularities responsible for the single peak in the optical conductivity are of the same M_1 type. These features can be used to find out the nature of the RSOI experimentally.

This paper is organized as follows. In section II, we describe basic properties of the 2DEG with anisotropic k-cubic spin-orbit interaction. In section III, we present the analytical and numerical results of the Drude weight and the optical conductivity. The summary and conclusions of this paper are presented in section IV.

II. DESCRIPTION OF THE PHYSICAL SYSTEM

The effective Hamiltonian of the electron in d_{xz} and d_{yz} orbitals at the interface of $LaAlO_3/SrTiO_3$ is given by[22]

$$H = \frac{\hbar^2\mathbf{k}^2}{2m^*} + \alpha(k_x^2 - k_y^2)(\mathbf{k}\times\boldsymbol{\sigma})\cdot\hat{z}, \tag{1}$$

where m^* is the effective mass of the electron, α is the strength of the anisotropic RSOI and $\boldsymbol{\sigma} = \sigma_x\hat{x} + \sigma_y\hat{y}$. The anisotropic dispersion relations and the corresponding eigenfunctions are given by

$$E_\lambda(\mathbf{k}) = \frac{\hbar^2k^2}{2m^*} + \lambda\alpha k^3|\cos 2\theta| \tag{2}$$

and $\psi_{\mathbf{k}}^\lambda(\mathbf{r}) = e^{i\mathbf{k}\cdot\mathbf{r}}\phi_{\mathbf{k}}^\lambda(\mathbf{r})/\sqrt{\Omega}$ with the spinor

$$\phi_{\mathbf{k}}^\lambda(\mathbf{r}) = \frac{1}{\sqrt{2}}\begin{pmatrix}1\\ \lambda\eta_{\mathbf{k}} i e^{i\theta}\end{pmatrix}. \tag{3}$$

Here Ω is the surface area of the two-dimensional system, $\lambda = \pm$ denotes the spin-split branches and $\eta_{\mathbf{k}} = \cos 2\theta/|\cos 2\theta|$ with $\theta = \tan^{-1}(k_y/k_x)$ measures the anisotropy of the spectrum. The magnitude of the anisotropic spin-splitting energy is $E_g(\mathbf{k}) = |E_+(\mathbf{k}) - E_-(\mathbf{k})| = 2\alpha k^3|\cos 2\theta|$. The spin splitting energy vanishes at $\theta = (2p+1)\pi/4$ with $p = 0, 1, 2, 3$. On the other hand, the maximum spin-splitting ($E_g^{\max} = 2\alpha k^3$) occurs at $\theta = p\pi/2$. To allow only the bound states, the wave-vector $\mathbf{k}$ should have an upper cut-off given by $k_c(\pi/4) = \hbar^2/(3m^*\alpha)$ which corresponds to the cut-off energy $E_c = \alpha k_c^3/2$.

The spin texture on the k_x-k_y plane can be obtained from the average values of spin vector (in units of $3\hbar/2$) $\mathbf{P}_\lambda(\mathbf{k}) = \langle\boldsymbol{\sigma}\rangle_\lambda = \lambda\eta_{\mathbf{k}}\hat{\theta}$, where $\hat{\theta} = -\hat{x}\sin\theta + \hat{y}\cos\theta$ is the unit polar vector. The electron spin lies in the $\mathbf{k}$ plane and always locked at right angles to its momentum.

The Berry connection[29] is defined as $\mathbf{A}_{\mathbf{k}} = i\langle\phi_{\mathbf{k}}^\lambda|\bigtriangledown_{\mathbf{k}}|\phi_{\mathbf{k}}^\lambda\rangle$, where $\phi_{\mathbf{k}}^\lambda$ is the spinor part of the wave function $\psi_{\mathbf{k}}^\lambda(\mathbf{r})$. The Berry connection for this system yields $\mathbf{A}_{\mathbf{k}} = -\hat{\theta}/(2k)$. Using the expression of the Berry phase[29] $\gamma = \oint\mathbf{A}_{\mathbf{k}}\cdot d\mathbf{k}$, we get $\gamma_{\rm ani} = -\pi$ for anisotropic case, whereas $\gamma_{\rm iso} = 3\pi$ for isotropic cubic RSOI[30].

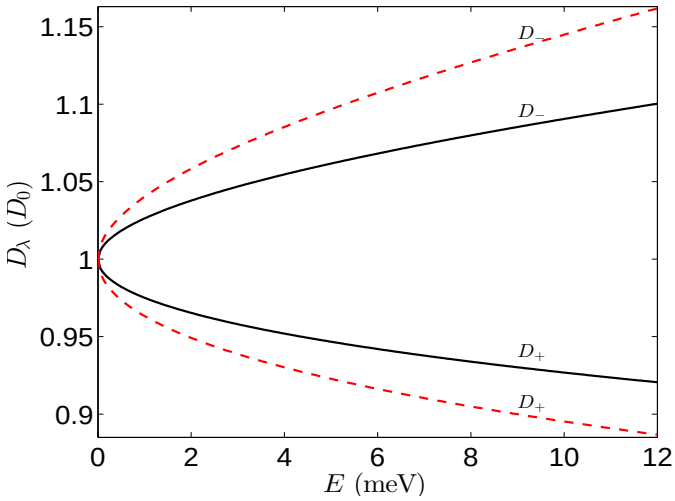

FIG. 1: (color online) Plots showing the density of states in the units of D_0 for two different values of α. Here $\alpha = 0.004$ eV nm^3 (solid black) and $\alpha = 0.006$ eV nm^3 (dotted red).

In order to obtain two anisotropic Fermi contours $k_f^\lambda(\theta)$, we need to calculate density of states (DOS) and Fermi energy E_f. The density of states of the spin-split energy branches are given by

$$\begin{aligned} D_\lambda(E) &= \int\frac{d^2k}{(2\pi)^2}\delta(E - E_\lambda(\mathbf{k})) \\ &= \frac{D_0}{2\pi}\int_0^{2\pi}\frac{k_E^\lambda(\theta)\,d\theta}{|k_E^\lambda(\theta) + \lambda 6\pi\alpha D_0(k_E^\lambda(\theta))^2|\cos 2\theta||}, \end{aligned}$$

where $D_0 = 2\pi m^*/h^2$ and $k_E^\lambda(\theta)$ being the solution of the equation $(\hbar k_E^\lambda)^2/2m^* + \alpha\lambda(k_E^\lambda)^3|\cos 2\theta| - E = 0$. The density of states is obtained numerically and their characteristics for the two branches are shown in Fig. 1. The DOS of the anisotropic spin-split levels varies asymmetrically with respect to D_0. For fixed electron density n_e and α, the Fermi energy (E_f) is obtained from the conservation of electron number $n_e = \int_0^{E_f}\sum_\lambda D_\lambda(E)dE$. The variations of the Fermi energy with n_e and α are shown in Fig. 2. The Fermi energy increases with the increase

of the carrier density. On the other hand, the Fermi energy decreases with the increase of the spin-orbit coupling strength. The Fermi wave vectors $k_f^\lambda(\theta)$ can be obtained numerically from the solutions of the equation $\hbar^2k^2/2m^* + \lambda\alpha k^3|\cos 2\theta| - E_f = 0$. The Fermi contours are depicted in Fig. 5 (color: black).

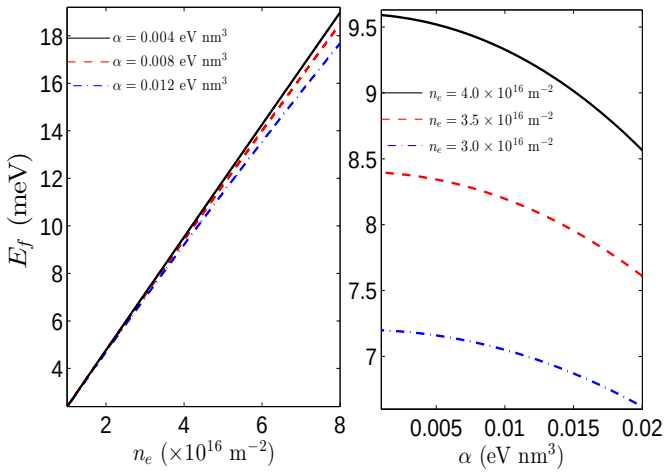

FIG. 2: (color online) Plots of the Fermi energy vs n_e and α. Left panel: plots of the Fermi energy vs density for different values of α. Right panel: plots of the Fermi energy vs α for different values of carrier density n_e.

III. DRUDE WEIGHT AND OPTICAL CONDUCTIVITY

The complex charge conductivity for a two-level system of charge carriers in presence of a sinusoidal electric field ($\mathbf{E}(\omega) \sim \hat{\mathbf{x}}E_0e^{i\omega t}$) can be written as $\Sigma_{xx}(\omega) = \sigma_D(\omega) + \sigma_{xx}(\omega)$, where $\sigma_D(\omega)$ is the intra-band induced dynamic Drude conductivity and $\sigma_{xx}(\omega)$ is the inter-band induced complex optical conductivity.

The absorptive part of the conductivity can be obtained by taking the real part of $\Sigma_{xx}(\omega)$ and is given by

$$\mathrm{Re}\left[\Sigma_{xx}(\omega)\right] = D_w\delta(\omega) + \mathrm{Re}\left[\sigma_{xx}(\omega)\right].$$

Here, D_w is known as the Drude weight measuring the Drude conductivity ($\sigma_d = \tau D_w/\pi$) for a DC electric field and $\mathrm{Re}\left[\sigma_{xx}(\omega)\right]$ is the optical conductivity as a function of the frequency of the AC electric field with vanishing momentum $q \to 0$. The vanishing momentum of the electric field forces the charge carriers to make a transition from $\lambda = -1$ branch to $\lambda = +1$ branch such that the momentum is conserved.

Drude weight: The semi-classical expression for the Drude weight at low temperature is given by[31]

$$D_w = \pi e^2 \sum_\lambda \int \frac{d^2\mathbf{k}}{(2\pi)^2} \langle\hat{v}_x\rangle_\lambda^2 \delta(E_\lambda(\mathbf{k}) - E_f). \qquad (4)$$

Here $\hat{v}_x$ is the x-component of the velocity operator. Using the Heisenberg's equation of motion, $i\hbar\dot{\mathbf{r}} = [\mathbf{r}, H]$, the x- and y-components of the velocity operator are given by

$$\hat{v}_x = \frac{\hbar k_x}{m^*}\mathbb{I} + \frac{\alpha}{\hbar}\left[(3k_x^2 - k_y^2)\sigma_y - 2k_xk_y\sigma_x\right] \qquad (5)$$

and

$$\hat{v}_y = \frac{\hbar k_y}{m^*}\mathbb{I} - \frac{\alpha}{\hbar}\left[(3k_y^2 - k_x^2)\sigma_x - 2k_xk_y\sigma_y\right]. \qquad (6)$$

For the system with anisotropic cubic RSOI, the calculation of the Drude conductivity yields

$$D_w^{\mathrm{ani}} = \left(\frac{e}{2\pi\hbar}\right)^2 \sum_\lambda \int_0^{2\pi} m^*[v_f^\lambda(\theta)]^2 B_\lambda(\theta) d\theta, \qquad (7)$$

where $v_f^\lambda(\theta) = \hbar k_f^\lambda(\theta)/m^*$ and

$$B_\lambda(\theta) = \frac{[\cos\theta + \lambda\eta_{\mathbf{k}}\alpha V_f^\lambda(\theta)(5\cos\theta + \cos 3\theta)/2]^2}{1 + \lambda 3\alpha V_f^\lambda(\theta)} \qquad (8)$$

with $V_f^\lambda(\theta) = (m^*/\hbar^2)k_f^\lambda(\theta)$.

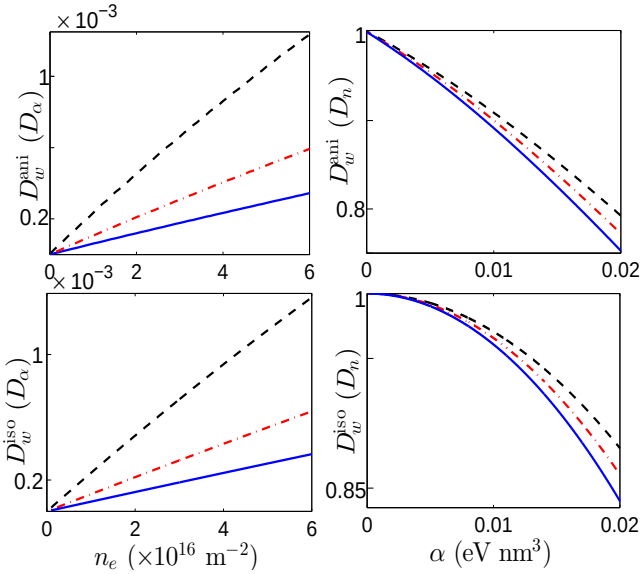

FIG. 3: (color online) Left panels: plots of the Drude weight D_w (in units of $D_\alpha = \pi e^2/m^*l_\alpha^2$) vs n_e for $\alpha = 0.006$ eV nm^3 (solid: blue), $\alpha = 0.008$ eV nm^3 (dotted-dashed: red) and $\alpha = 0.012$ eV nm^3 (dashed: black). Here $l_\alpha = m^*\alpha/\hbar^2$. Right panel: plots of D_w (in units of $D_n = \pi e^2 n_e/m^*$) vs α for $n_e = 3 \times 10^{16}$ m^{-2} (dashed: black), $n_e = 3.5 \times 10^{16}$ m^{-2} (doted-dashed: red) and $n_e = 4 \times 10^{16}$ m^{-2} (solid: blue).

For carrying out the numerical calculation, we adopt the following parameters used in Refs.[17,22]: $n_e = 3.5 \times 10^{16}$ m^{-2} and $m^*/m_0 = 1$, where m_0 is the bare mass of the electron. In Fig. 3, the variations of the Drude weight with the carrier density and with the strength of

the Rashba spin-orbit interactions are shown. The plots of the Drude weight vs carrier density for three different values of α are shown in the left panels of Fig. 3. The analytical expression of $D_w^{\rm iso}$ obtained in Ref.[30] clearly shows the deviation from the linear density dependence. Because of the small value of α considered here, the deviation is not visible in this figure. On the other hand, the Drude weight vs α for three different values of carrier density are plotted in the right panels of Fig. 3. The Drude weight decreases with the increase of α but the decreasing nature of D_w for the two different cases is quite different. This important feature would help to know the nature of the RSOI.

Optical Conductivity: The generalized Kubo formula of the optical conductivity in terms of the Matsubara Green's function is given by[31]

$$\sigma_{\mu\nu}(\omega) = -\frac{e^2T}{i\omega}\frac{1}{(2\pi)^2}\int d^2\mathbf{k} \times \sum_l {\rm Tr}\langle\hat{v}_\mu\hat{G}(\mathbf{k},\omega_l)\hat{v}_\nu\hat{G}(\mathbf{k},\omega_s+\omega_l)\rangle_{i\omega_s\to\omega+i\delta}. \quad (9)$$

Here, $\mu,\nu = x,y$, T being the temperature, $\omega_s = (2s+1)\pi T$ and $\omega_l = 2l\pi T$ are the fermionic and bosonic Matsubara frequencies with s and l are integers, respectively.

The matrix Green's function associated with the Hamiltonian given by Eq. (1) is

$$G(\mathbf{k},\omega_n) = \frac{1}{2}\sum_\lambda \Big[\mathbb{I} + \mathbf{P}_\lambda(\mathbf{k})\cdot\boldsymbol{\sigma}\Big]G_0^\lambda(\mathbf{k},\omega_n). \quad (10)$$

Here $\mathbb{I}$ is a 2×2 unit matrix and $G_0^\lambda(\mathbf{k},\omega_n) = 1/(i\hbar\omega_n + \mu_0 - E_\lambda(\mathbf{k}))$ with μ_0 being the chemical potential. It indicates that the optical spectral weight is directly related to the local spin texture $\mathbf{P}_\lambda(\mathbf{k})$.

Substituting Eqs. (5) and (10) into Eq. (9), the xx-component of the longitudinal conductivity reduces to

$$\sigma_{xx}(\omega) = -\frac{e^2}{i(2\pi\hbar)^2\omega}\int_0^\infty\int_0^{2\pi}\alpha^2k^5\cos^2 2\theta\sin^2\theta dk d\theta \times \Big[\frac{f(E_-)-f(E_+)}{\hbar\omega+i\delta-E_++E_-} + (E_-\leftrightarrow E_+)\Big], \quad (11)$$

where $f(E) = [e^{(E-\mu_0)\beta}+1]^{-1}$ is the Fermi-Dirac distribution function with $\beta = 1/(k_BT)$.

We have carried out the same calculation for other components of the conductivity tensor $\sigma_{\mu\nu}(\omega)$. We find that $\sigma_{yy}(\omega) = \sigma_{xx}(\omega)$ and $\sigma_{xy}(\omega) = \sigma_{yx}(\omega) = 0$. Hence the optical conductivity remains isotropic despite the fact that the Fermi contours are anisotropic.

Using the fact that $\omega > 0$ and after performing the k integral, the expression for the absorptive part of the optical conductivity at $T = 0$ is given by

$${\rm Re}\,[\sigma_{xx}(\omega)] = \frac{e^2}{24h}\int_0^{2\pi}d\theta\sin^2\theta\Big[\Theta(\mu_+)-\Theta(\mu_-)\Big], \quad (12)$$

where $\Theta(x)$ is the unit step function and $\mu_\pm = E_\pm(k_\omega) - \mu_0$ with $k_\omega \equiv k_w(\theta) = (\hbar\omega/2\alpha|\cos 2\theta|)^{1/3}$. This integral can not be solved analytically due to θ dependence of k_ω.

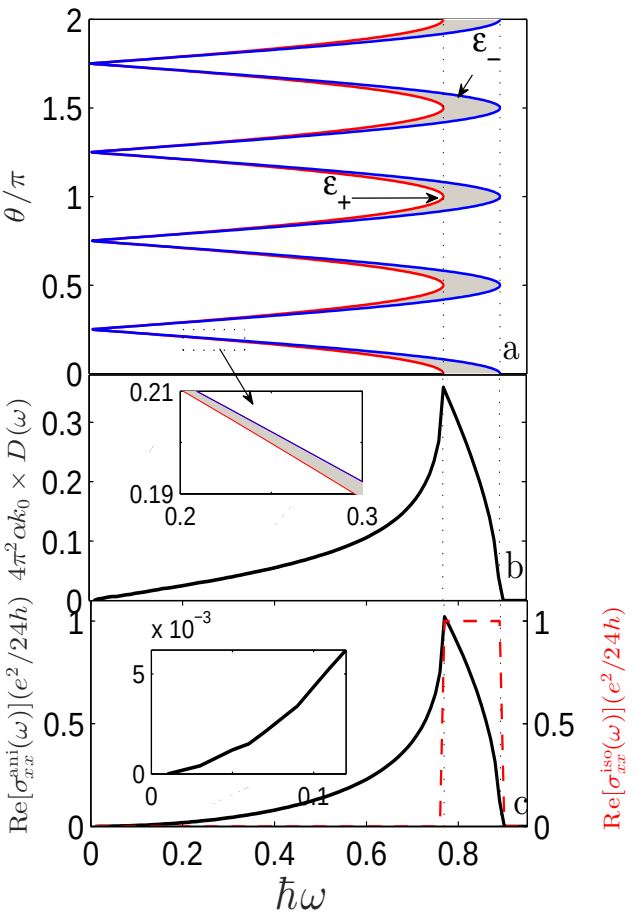

FIG. 4: (color online): Top panel: Plots of $\epsilon_\pm(\theta)$ vs θ. Middle panel: plots of the joint density of states vs $\hbar\omega$ with $k_0 = \sqrt{2\pi n_e}$. Bottom panel: the real part of the optical conductivity as a function of photon energy $\hbar\omega$.

On the other hand, in isotropic cubic Rashba SOC the closed form expression of the absorptive part of the optical conductivity at $T = 0$ K is given by[30]

$${\rm Re}\,[\sigma_{xx}^{\rm iso}(\omega)] = \frac{3e^2}{16\hbar}\big[\Theta(\tilde{\mu}_+)-\Theta(\tilde{\mu}_-)\big], \quad (13)$$

where $\tilde{\mu}_\pm = E_\pm(\tilde{k}_\omega) - \mu_0$ with $\tilde{k}_\omega = (\hbar\omega/2\alpha)^{1/3} = k_w(\theta = (2p+1)\pi/2)$. It leads to featureless optical conductivity which has box shape with the height $\sigma_{xx}^{\rm iso} = 3e^2/(16\hbar)$ which is independent of the carrier density and α. Note that simultaneous presence of isotropic Rashba and Dresselhaus SOI leads to anisotropic Fermi contours, in turns produces interesting optical features. Whereas anisotropic RSOI alone gives rise to anisotropic Fermi contours and provides distinct optical features.

Here we shall present how the anisotropic RSOI alone gives rise to some unique features of the optical conductivity. We first evaluate ${\rm Re}\,[\sigma_{xx}(\omega)]$ numerically using the parameters $\alpha = 0.004$ eV nm^3, $n_e = 3.5\times10^{16}$ m^{-2} and $m^*/m_0 = 1$ as used in Refs.[17,22] and shown in the

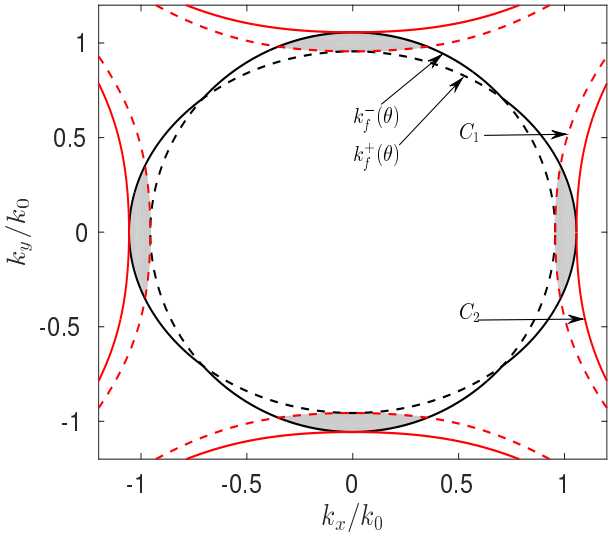

FIG. 5: (color online) Plots of the Fermi contours $k_f^+(\theta)$, $k_f^-(\theta)$, the constant-energy difference curves C_1: $E_g(\mathbf{k}) = \epsilon_1$ and C_2: $E_g(\mathbf{k}) = \epsilon_2$.

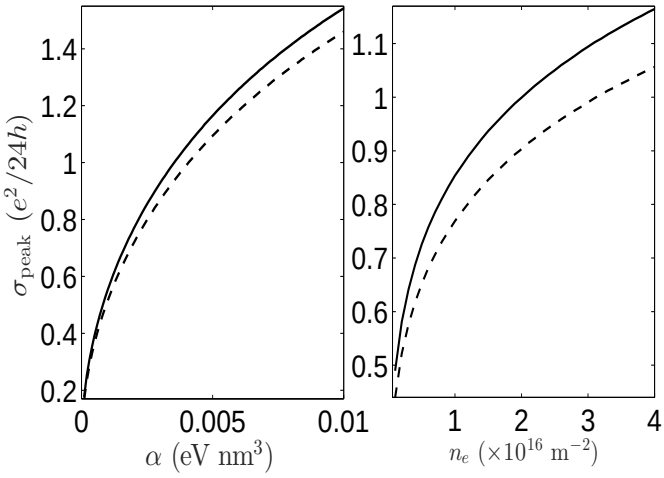

FIG. 6: (color online) Left panel: Plots of $\sigma_{\rm peak}$ vs α for fixed values of $n_e = 4.0 \times 10^{16}$ m^{-2} (dashed) and $n_e = 3.0 \times 10^{16}$ m^{-2} (solid). Right panel: Plots of $\sigma_{\rm peak}$ vs n_e for different values of $\alpha = 0.004$ eV nm^3 (solid) and $\alpha = 0.006$ eV nm^3 (dashed).

lower panel of Fig. 4. For comparison with the isotropic case, we plot Re $[\sigma_{xx}^{\rm iso}(\omega)]$ which appears as the rectangular box on the right side of the lower panel of Fig. 4. We depict $\epsilon_\pm(\theta) = 2\alpha[k_f^\pm(\theta)]^3|\cos(2\theta)|$ in the top panel of Fig. 4. The contribution to optical conductivity arises from the shaded angular region. The optical transitions from $\lambda = -1$ to $\lambda = +1$ occur when the photon energy satisfies the inequality $0 < \hbar\omega < \epsilon_-(\theta)$. One can see that an infinitesimally small photon energy can initiate the optical transition, in complete contrast to the isotropic SOI case. This is due to the presence of the degenerate lines $\theta = (2p+1)\pi/4$. There is a single peak of the Re $[\sigma_{xx}(\omega)]$ at $\hbar\omega = \epsilon_+(p\pi/2) = 2\alpha[k_f^+(p\pi/2)]^3$ and the optical conductivity becomes zero when $\hbar\omega \geq \epsilon_-(p\pi/2) = 2\alpha[k_f^-(p\pi/2)]^3$. For better understanding of these features, we plot the constant energy-difference curves $E_g(\mathbf{k}) = \epsilon_\omega$ for $\epsilon_\omega = \epsilon_+(p\pi/2) = \epsilon_1$ (C_1: dashed) and $\epsilon_\omega = \epsilon_-(p\pi/2) = \epsilon_2$ (C_2: solid) in Fig. 5. The area intercept by the curves C_i with $i = 1, 2$ and the Fermi contours (k_f^λ) are responsible for the **k**-selective optical transitions as shown in Fig. 5.

The overall behavior of the optical spectra can be understood from the joint density of states which is given as

$$D(\omega) = \int \frac{d^2\mathbf{k}}{(2\pi)^2}[f(E_+(\mathbf{k})) - f(E_-(\mathbf{k}))]\delta(E_g(\mathbf{k}) - \hbar\omega).$$

It can be reformulated as

$$D(\omega) = \frac{1}{(2\pi)^2}\int_C \frac{dC[f(E_+(k_\omega)) - f(E_-(k_\omega))]}{|\partial_k E_g(\mathbf{k})|_{E_g=\hbar\omega}}. \quad (14)$$

Here C is the line element along the contour. The joint density of states vs $\hbar\omega$ is plotted in the middle panel of

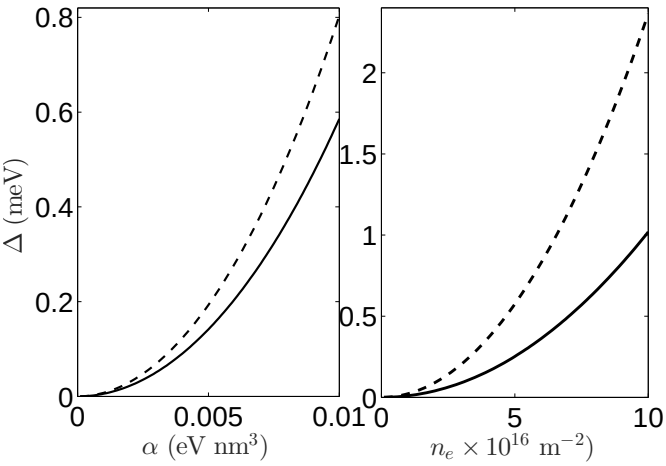

FIG. 7: (color online) Left panel: Plots of Δ vs α for fixed values of $n_e = 3.5 \times 10^{16}$ m^{-2} (dashed) and $n_e = 3.0 \times 10^{16}$ m^{-2} (solid). Right panel: Plots of Δ vs n_e for different values of $\alpha = 0.004$ eV nm^3 (solid) and $\alpha = 0.006$ eV nm^3 (dashed).

Fig. 4. The location of the single peak and the region of zero optical conductivity are nicely described by the joint density of states. It can be seen from Eq. (14) that any peak may arise whenever $|\partial_k E_g(\mathbf{k})|$ attains a minimum value. For the present problem, the singular points are at $\mathbf{k}_s = (k, p\pi/4)$. The single peak appears at $\epsilon_\omega = \epsilon_-(p\pi/2)$ in the joint density of states correspond to the well known van Hove singularity. The asymmetric

spin-splitting at the Fermi contours along the $k_y = k_x = 0$ lines is the reason for the appearance of the peak at $\epsilon_-(p\pi/2)$.

There are three different types of the singularity[32] depending on the nature of change of the energy gap around the singular points $\mathbf{k}_s$. Using the Taylor series expansion of $E_g(\mathbf{k})$ around $\mathbf{k}_s$ as $E_g(\mathbf{k}) = E_g(\mathbf{k}_s) + \sum_\mu a_\mu(p)(k_\mu - k_{s\mu})^2$ with the expansion coefficients $2a_\mu(p) = \frac{\partial^2 E_g(\mathbf{k})}{\partial k_\mu^2}\Big|_{\mathbf{k}_s}$. The co-efficients a_μ are as follows $a_x(p) = \alpha k[5+7(-1)^p]$ and $a_y(p) = \alpha k[5-7(-1)^p]$. The sign of the coefficients will determine the type of classification of the various singular points. One can easily find that the signs of a_x and a_y at different singular points are $(-1)^p$ and $(-1)^{p+1}$, respectively. Therefore, every singularities are all of the same class i.e. M_1 type.

The variations of the peak height ($\sigma_{\rm peak}$) with n_e and α are shown in Fig. 6. It strongly depends on the Fermi energy. We also define a width $\Delta = \epsilon_-(p\pi/2) - \epsilon_+(p\pi/2)$, the difference between peak position and the position beyond which $\sigma_{xx}(\omega)$ vanishes. Its variation with α as well as n_e are shown in Fig. 7. It shows that Δ increases with the increase of n_e as well as α.

IV. SUMMARY AND CONCLUSION

We have studied the Drude weight and optical conductivity for 2DEG with k-cubic anisotropic RSOI at the oxide interface. We have presented the variation of the zero-frequency Drude weight with the carrier density as well as the strength of the anisotropic spin-orbit coupling. For anisotropic RSOI, the Drude weight deviates from the linear density dependence. It is indicated that the spectral weight is directly related to the local spin texture in momentum space. We found that the charge and optical conductivities remain isotropic although the Fermi contours are anisotropic. It is found that an infinitesimally small photon energy can trigger inter-band optical conductivity. This is due to the fact that the spin-splitting energy vanishes along the certain directions in $\mathbf{k}$ space. We found a single peak in the optical conductivity whose value depends on the Fermi energy. We have shown that the van Hove singularities responsible for the single peak in the optical conductivity are of the same M_1 type. The different features of the conductivity can determine the information of the nature of the spin-orbit interaction experimentally and would help in understanding the orbital origin of the two-dimensional electron gas at the oxide interface.

[1] R. Winkler, Spin-orbit Coupling Effects in Two-Dimensional Electron and Hole systems (Springer, Berlin 2003).
[2] I. Zutic, J. Fabian, and S. Das Sarma, Rev. Mod. Phys. **76**, 323 (2004).
[3] E. I. Rashba, Sov. Phys. Solid State **2**, 1109 (1960).
[4] Y. A. Bychkov and E. I. Rashba, J. Phys. C: Solid State Phys. **17**, 6039 (1984).
[5] G. Dresselhaus, Phys. Rev. **100**, 580 (1955).
[6] B. Das, D. C. Miller, S. Datta, R. Reifenberger, W. P. Hong, P. K. Bhattachariya, J. Sing, and M. Jaffe, Phys. Rev. B **39**, 1411 (1989); J. Nitta, T. Akazaki, H. Takayanagi, and T. Enoki, Phys. Rev. Lett. **78**, 1335 (1997).
[7] M. Z. Hasan and C. L. Kane, Rev. Mod. Phys. **82**, 3045 (2010); X. L. Qi and S. C. Zhang, Rev. Mod. Phys. **83**, 1057 (2011); Y. Xu, I. Miotkowski, C. Liu, J. Tian, H. Nam, N. Alidoust, J. Hu, Chih-Kang Shih, M. Z. Hasan, and Y. P. Chen, Nature Phys. **10**, 956 (2014).
[8] E. I. Rashba and E. Ya. Sherman, Phys. Lett. A **129**, 175 (1988).
[9] R. Winkler, Phys. Rev. B **62**, 4245 (2000); G. M. Minkov, A. A. Sherstobitov, A. V. Germanenko, O. E. Rut, V. A. Larionova, and B. N. Zvonkov, Phys. Rev. B **71**, 165312 (2005).
[10] H. Nakamura, T. Koga, and T. Kimura, Phys. Rev. Lett. **108**, 206601 (2012).
[11] R. Moriya, K. Sawano, Y. Hoshi, S. Masubuchi, Y. Shiraki, A. Wild, C. Neumann, G. Abstreiter, D. Bougeard, T. Koga, and T. Machida, Phys. Rev. Lett. **113**, 086601 (2014).
[12] A. Ohtomo and H. Y. Hwang, Nature. **427**, 423 (2004).
[13] A. D. Caviglia, S. Gariglio, N. Reyren, D. Jaccard, T. Schneider, M. Gabay, S. Thiel, G. Hammerl, J. Mannhart, and J.-M. Triscone, Nature. **456**, 624 (2008).
[14] C. Bell, S. Harashima, Y. Kozuka, M. Kim, B. G. Kim, Y. Hikita, and H. Y. Hwang, Phys. Rev. Lett **103**, 226802 (2009).
[15] G. K. B. Lee and A. H. MacDonald, Phys. Rev. B **88**, 041302 (2013).
[16] Z. S. Popovic, S. Satpathy, and R. M. Martin, Phys. Rev. Lett. **101**, 256801 (2008).
[17] Z. Zhong, A. Toth, and K. Held, Phys. Rev. B **87**, 161102(R) (2013).
[18] G. Khalsa, B. Lee, and A. H. MacDonald, Phys. Rev. B **88**, 041302 (2013).
[19] Y. Kim, R. M. Lutchyn, and C. Nayak, Phys. Rev. B **87**, 245121 (2013).
[20] L. W. van Heeringen, G. A. de Wijs, A. McCollam, J. C. Maan, and A. Fasolino, Phys. Rev. B **88**, 205140 (2013).
[21] C. Cancellieri, M. L. Reinle-Schmitt, M. Kobayashi, V. N. Strocov, P. R. Willmott, D. Fontaine, Ph. Ghosez, A. Filippetti, P. Delugas, and V. Fiorentini, Phys. Rev. B **89**, 121412(R) (2014); P. D. C. King, S. M. Walker, A. Tamai, A. de la Torre, T. Eknapakul, P. Buaphet, S.-K. Mo, W. Meevasana, M. S. Bahramy, and F. Baumberger,

Nat. Commun. **5**, 3414 (2014).
[22] J. Zhou, W. Shan, and D. Xiao, Phys. Rev. B **91**, 241302(R) (2015).
[23] L. Li, C. Richter, J. Mannhart, and R. C. Ashoori, Nat. Phys. **7**, 762 (2011).
[24] J. A. Bert, B. Kalisky, C. Bell, M. Kim, Y. Hikita, H. Y. Hwang, and K. A. Moler, Nat. Phys. **7**, 767 (2011).
[25] W. Xu and L. B. Lin, J. Phys.: Condens. Matter **16**, 1777 (2008).
[26] C. H. Yang, W. Xu, Z. Zeng, F. Lu, and C. Zhang, Phys. Rev. B **74**, 075321 (2006).
[27] A. Wong and F. Mireles, Phys. Rev. B **81**, 085304 (2010).
[28] Z. Li, F. Marsiglio, and J. P. Carbotte, Sci. Rep. **3**, 2828 (2013).
[29] M. V. Berry, Proc. R. Soc. London, Ser. A **392**, 45 (1984).
[30] A. Mawrie and T. K. Ghosh, arXiv: 1511:04917
[31] G. D. Mahan, Many Particle Physics, (Springer Science, New York-1981).
[32] C. Hamaguchi, Basic Semiconductor Physics, (Springer-Verlag-2010).